# Numerical Simulation of Dilatation Patterns of the Ascending Aorta in Aorthopaties

Diana Marta Cruz de Oliveira

*IST, Universidade de Lisboa, Portugal*

June 24, 2016

**Abstract**

Aortic dilation (AD) is associated with the congenital bicuspid aortic valve (BAV) disease and with the genetic Marfan Syndrome (MFS) disorder. Although the main cause for AD in MFS is aortic wall weakening, in BAV disease this is still not completely understood. In this work, we consider blood hemodynamics in BAV patients with different AD and aortic regurgitation (AR), and in an MFS patient with dilated aortic root, in comparison with a healthy aorta. A fluid-structure interaction numerical approach is implemented regarding patient-specific geometries, where the aortic valves are defined by analytical orifices. Results show that, while the healthy aorta displayed a typical hemodynamic behavior of flows in bends, BAV related aortas present an accelerated flow along the outer aortic wall. Wall shear stress (WSS) overload in the outer curvature was observed, more marked in more dilated aortas. Moreover, helices in the ascending aorta (AA) were present in all BAV patients, enhanced with greater dilation. These findings support that hemodynamic factors play an important role in AD formation and development in BAV patients, caused by a prolonged exposure of the outer AA curvature to altered WSS. Alternatively, greater regurgitation was associated with abnormal WSS distributions in the AA during diastole, showing that severe AR can facilitate aortic root dilation. Moreover, the MFS patient presented very low WSS in the dilated root, a condition observed in intracranial aneurysms. Numerical modeling can therefore provide important biomarkers for the description of the hemodynamic environment in several aortic pathologies, hence guiding preventive medical intervention.

**Keywords:** Ascending aorta, Bicuspid aortic valve, Marfan Syndrome, Computed Tomography, Fluid-Structure Interaction, Numerical Simulation

## 1. Introduction

The cardiovascular system is extremely complex. The heart, central organ of this system, functions as a mechanical cycling pump, pumping blood to the entire body. In the left part of the heart, the left ventricle pumps oxygenated blood throughout the arterial tree across the most important artery in the human body – the aorta. It possesses special biomechanical properties which allow it to adapt to the stress imposed by turbulent blood flow while passing through the aortic valve: the mobility, elasticity and structural integrity of both the valve cusps and the ascending aortic wall are essential to a good functioning of the cardiovascular system (Tilea et al., 2013).

However, with aging, harmful changes in the aortic wall architecture, namely loss of compliance and aortic dilation (AD), occur, giving rise to arterial pressure and blood velocity increase, which results in a decrease in organ perfusion (Tilea et al., 2013; Erbel et al., 2006). Moreover, some cardiovascular pathologies can cause a faster and/or abnormal rate on this type of aorthopaties. Over the past few decades, AD has been highly associated with the congenital bicuspid aortic valve (BAV) and with the genetic Marfan Syndrome (MFS), being a key risk factor for aortic rupture, a major cardiovascular cause of morbidity and mortality (Kang et al., 2013; Aburawi et al., 2007).

In MFS, AD (more prevalent in the aortic root) affects at least 80% of the adult population by the age of 40 (Aburawi et al., 2007). It arises from a genetic defect on the aortic wall that causes it to be thinner and weaker, therefore not being able to sustain physiological hemodynamic stress (Erbel et al., 2006). Alternatively, in BAV patients, AD is a quite heterogeneous aortopathy (Kang et al., 2013). BAV is a congenital heart malformation, more frequent in male sex, characterized by a valve formed by two leaflets instead of three (Kang et al., 2013). Additionally, it is highly associated with diverse complications such as aortic regurgitation (AR) and aortic stenosis (AS) (Erbel et al., 2006; Kang et al., 2013).

AD related with BAV starts developing during childhood, evolving through life and affecting from about 20 to 85% of the adult BAV population (Kang et al., 2013). Its etiology remains unclear and current evidence suggests that it results from the interaction between genetic and hemodynamic factors: a genetic predisposition in patients with a BAV might cause an intrinsic aortic wall abnormality, which confers susceptibility for AD, and the presence of altered hemodynamics observed in BAV patients acts as a triggering and maintaining factor of that dilation, especially in the ascending aorta (AA) (Hope et al., 2010).

In BAV patients, abnormal flow characterized as asymmetric and with nested right- or left-handed helices in the AA has been documented (Hope et al., 2010). Even though helical flows have been observed in both healthy and dilated BAV associated aortas (Hope et al., 2010), strong correlations between blood flow asymmetrical jet angles and aortic diameters have been found, suggesting that larger aortic diameters are associated to larger angles of misdirected flow (Reijer et al., 2010).

Eccentric flow in BAV has been reported by distinct techniques, such as echocardiography, four-dimensional flow and phase-contrast magnetic resonance imaging (Hope et al., 2010), and computational studies (Viscardi et al., 2010; Faggiano et al., 2012; Pasta et al., 2013; Rinaudo et al., 2014, Cao et al., 2015).

### 1.1. Computational studies

Computational studies confirmed the results obtained from imaging studies – in addition, they have shown that asymmetrical flow jets in BAV are correlated with an increase in peak velocity in systole and elevated viscous stresses exerted by the blood on the aortic wall (Viscardi et al., 2010) - wall shear stress (WSS) - in the AA. This was verified in both healthy (Viscardi et al., 2010) and dilated aortas and, in the latter, a connection between high WSS values and the dilated wall was observed (Faggiano et al., 2012; Pasta et al., 2013). In fact, it has been stated that abnormal flow initiates AD as a compensatory response to keep constant WSS through vascular remodeling (Reijer et al., 2010). Furthermore, dependence of the flow patterns and the WSS distribution on the BAV fusion type were observed (Viscardi et al., 2010; Cao et al., 2015). Alternatively, computational studies regarding MFS patients have shown local helicity in the AA, and, in dilated aortic roots, low velocity recirculation areas associated with low WSS were observed (Singh et al., 2016).

Deeper insight on the formation and development of blood flow patterns in the AA in BAV and MFS patients needs to be provided. Moreover, computational studies of the association between AD and AR in BAV cases have not been made. Alternatively, almost no computational studies have been performed to study aortic hemodynamics in MFS patients with AD. In this work, we try to provide further understanding on blood hemodynamics in non-stenotic BAV patients with different degrees of AA dilation, as well as in an MFS patient with dilated aortic root. Moreover, a preliminary qualitative assessment of the impact of AR on AA hemodynamics in diastole, when associated with BAV and AD, is made.

## 2. Methods

### 2.1. Patient dataset

Data concerning 82 patients with BAV, one patient with MFS and one healthy patient (9 years old with no valve conditions) were provided and analyzed. Aortic root dilation was defined as having an annulus' diameter greater than 36 mm and AA dilation as having a diameter greater than 35 mm[14]. Three BAV patients with different degrees of AD and one with severe AR were selected for consecutive computational analysis. All patients presented a non-stenotic right-left fusion type BAV, although patient K possessed an almost mildly stenotic BAV. In Table 1, additional information and aortic diameters are provided.

### 2.2. Image segmentation and geometry reconstruction

For each patient, high resolution thorax computed tomography (CT) images were provided from Hospital de Santa Marta (Centro Hospitalar de Lisboa Central), in DICOM format. All image studies were obtained without the application of endovenous, except for patient M.

Patient-specific (PS) aortic surface models were created through image segmentation of the lumen by using 3D Slicer (https://www.slicer.org/). Only the main aortic vessel and supra-aortic arteries (innominate, left common carotid and left subclavian arteries) were segmented, with the models originating at the mid-aortic root and extending to the middle of the descending aorta (DA).

The reconstructed surface model, in .stl format, was then repaired and smoothed in MeshLab (http://meshlab.sourceforge.net/). Afterwards, to design FSI aortic models, an open-source tool for PS fluid-structure vessel mesh generation developed in LifeV (http://www.lifev.org) by Elena Faggiano in Politecnico di Milano was used to generate the aortic wall from the vessel interface surface previously obtained. This tool, which aggregates methods available in the Vascular Modeling Toolkit (vmtk - http://www.vmtk.org/) with ad-hoc algorithms, receives as input a capped-ends interface surface file and generates two tetrahedral meshes, in .mesh format (fluid and solid domains). Since aortic wall thickness varies according to the radius of the lumen, a radius dependent meshing scheme was chosen according to data correlating aortic thickness and lumen diameter and, regarding patient K, a constant thickness of 1.6 mm was applied on his AA only.

Then, and after file conversion from .mesh to .stl using Gmsh (http://gmsh.info/), the aortic wall surface file suffered surface decimation using MeshLab and subsequent file conversion from .stl to .igs took

Table 1 – Patient clustering for AD and AR. Patients L (which presents coarctation in the aortic arch), M and T have non-stenotic R-L fusion type BAV, while patient K presents progressive mild AS.

| Patient | Age [years-old] / Gender [M/F] | Aortic dilation | Aortic coarctation | Aortic regurgitation | Aortic root diameter [mm] | AA diameter [mm] |
|---|---|---|---|---|---|---|
| **K** | 25 / M | Root + AA | No | Mild | 42 | 50 |
| **L** | 34 / M | Without | Yes | Mild | 28 | 30 |
| **M** | 33 / M | AA | No | Mild | 36 | 38.6 |
| **T** | 35 / M | Without | No | Severe | 26 | 30 |
| **MFS** | 24 / M | Root | Yes | None | 46 | ---- |

place using SolidWorks 2010 (http://www.solidworks.com/).

## 2.3. Numerical simulations

### 2.3.1. Aortic geometry preparation

To perform numerical simulations using COMSOL Multiphysics (https://www.comsol.com/), additional geometry post-processing features were made in COMSOL: first, re-scaling of the geometry was made to match realistic PS aortic dimensions; second, an analytical model of a BAV anatomic orifice was mathematically defined (Viscardi et al., 2010): the orifice was designed in a two-dimensional plane by the intersection of two circle functions with radius of 14.005 mm and 11.0033 mm, respectively, yielding an orifice area of about 2 $cm^2$ which was sampled into each aortic inlet. Moreover, a circular orifice was sampled at the inlet of the MFS patient in a similar way to what was done in (Singh et al., 2016).

### 2.3.2. Physics and boundary conditions

Six FSI numerical simulations were carried on for all aortic models in COMSOL. Blood was approximated as an incompressible, homogeneous and Newtonian fluid (density: 1050 $kg/m^3$; viscosity: 0.004 Pa*s) and the aortic wall was modeled as an isotropic, linear and elastic material. For all patients, values of density equal to 1120 $kg/m^3$ and Poisson's ratio equal to 0.45 were prescribed, while Young's modulus varied: values of 4.48 MPa, 4 MPa and 2 MPa were assigned for patient K, for the MFS patient and for the remaining patients, respectively.

For the inlet, physiological flow rate curves for TAV, BAV with mild AR and severe AR were considered (Figure 1) and five different velocity curves obtained by dividing the inflow rate by the inlet area were prescribed: for the healthy and MFS patients, the TAV velocity curve maintained unaltered; for the BAV patients M, K and L, the curves were re-scaled to match PS peak systolic velocities of 2.51 m/s, 1.41 m/s and 1.63 m/s, respectively; for the BAV patient T, the severe AR curve suffered no further alterations. Since the main goal of this work is to analyze the hemodynamics during systole, valve leaflets are not modeled, because it has been shown that the valve orifice shape in BAV configurations associated with the format of the aorta are sufficient to recreate related hemodynamic abnormalities (Faggiano et al., 2012). Moreover, valve leaflets strongly influence blood hemodynamics during diastole due to valve closing. Although the use of the GOA is not accurate for the diastole, we can still get qualitative information during this period. Therefore, inflow conditions have into account physiological aspects of a full cardiac cycle (systole and diastole) and are applied as a plug profile.

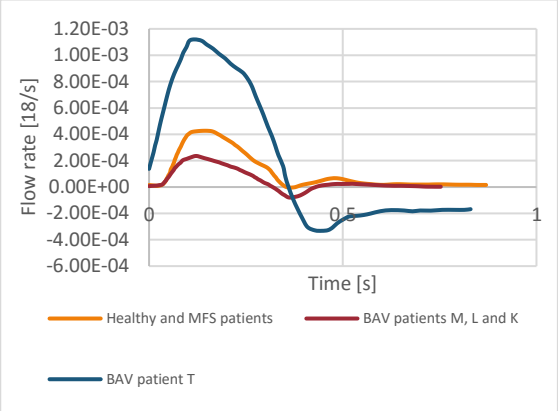


Figure 1 - Flow rate curves for the healthy patient and the MFS patient (Olufsen et al., 2000), for BAV patients K, L and M (adapted from (Barker et al., 2010; Nagel et al., 2004)) and BAV patient T (Nagel et al., 2004).

At the outlets, linear absorbing conditions in the form of pressure were prescribed. These work by applying, at a certain time step, an average pressure based on the flow rate at the previous time step that exits a certain outlet boundary (Janela et al., 2010). Additionally, the aortic wall was constrained in the axial direction at the inlet and outlet sections, a no-slip condition was imposed between blood and wall and a linear elastic support with a foundation stiffness of 75 mmHg/mm was applied on the outer aortic wall to account for the damping effect generated by the surrounding tissues on the aorta.

### 2.3.3. Computational approach

The FSI physics solved by COMSOL consisted of the momentum and continuity equations in the Arbitrary Lagrangian-Eulerian (ALE) formulation for the fluid (blood) and of the wall deformation equation in the Lagrangian form for the structure (aortic wall). All

governing equations were solved using the finite element method. A fully-coupled approach with the use of Newton-Raphson method (with damping) and the direct linear solver PARDISO was chosen for system equation solving. A time dependent study based on a second-order backward differentiation formula was selected. The initial time step was 0.001 seconds and the maximum allows time step was 0.004 seconds. All simulations but the one regarding patient T are carried out over three cardiac cycles to achieve temporal convergence, and the one for patient T was performed for two cardiac cycles, with the results being retrieved from the last cycle.

A finite element P1+P1 discretization with consistent stabilization methods was employed. The aortic wall and lumen were meshed using mostly tetrahedral elements, but prism, triangular, quadrilateral, edge and vertex ones were also used. A mesh sensitivity analysis was performed on the healthy patient's geometry, in a stationary physics, to choose the appropriate mesh density for the fluid domain. This analysis consisted of measuring the differential error in the obtained velocity solutions under increasing mesh density, through the use of the $H^1(\Omega)$ semi-norm and the $L^2(\Omega)$ norm. The initial coarse mesh was based on a maximum element size of 1.56 mm and a minimum element size of 1.41 mm for both fluid and solid domains, consisting of 334274 elements. Mesh refinement was achieved by progressively decreasing the maximum and minimum element sizes of the fluid domain mesh up to a final decrease of about 45%. A decrease in the error of the results was observed with increasing mesh refinement. An acceptable window of values appeared after about one million degrees of freedom (DOF) for the fluid domain, which is equivalent to a $L^2(\Omega)$ norm below about 3% and a $H^1(\Omega)$ semi-norm between 10% and 15%. However, and having into account computational costs, mesh and DOF were set accordingly to Table 2:

Table 2 – Mesh and DOF settings.

| Patient | Nº mesh elements | DOF (fluid domain) | DOF (solid domain) |
|---|---|---|---|
| **Control** | 620175 | 457852 | 1100694 |
| **K** | 427127 | 306764 | 820215 |
| **L** | 333236 | 340572 | 765456 |
| **M** | 498881 | 362800 | 802968 |
| **T** | 434501 | 326720 | 680826 |
| **MFS** | 486933 | 351548 | 832137 |

The simulations required between 5 and 9 days of computing time in a workstation with 64 RAM Gigabytes.

### 2.4. Hemodynamics characterization

Aortic hemodynamics was assessed in terms of velocity, fluid streamlines, helicity and WSS. Results were captured during the systolic peak, deceleration phase, late systole and late diastole. The spatial variations of the velocity profile along the streamwise direction are explored by depiction of the local velocity field over two cross-sections situated in the AA region, namely in the middle and distal segments.

Additionally, WSS magnitude was computed. In Newtonian fluids, we have

$$\mathrm{WSS} = \sigma_n - (\sigma_n \cdot n)n = \tau_n - (\tau_n \cdot n)n, \quad (1)$$

where $\tau_n$ is the viscous stress, given by

$$\tau_n = [\mu((\nabla u)^T + \nabla u)] \cdot n \quad (2)$$

where $\mu$ represents blood viscosity and $u$ is the velocity vector. The WSS temporal characteristics were also quantified in terms of time-averaged WSS (TAWSS),

$$\mathrm{TAWSS} = \frac{1}{T}\int_0^T \left|\overrightarrow{\mathrm{WSS}}\right| \, dt, \quad (3)$$

where $T$ is the cardiac period, and the oscillatory shear index (OSI),

$$\mathrm{OSI} = \frac{1}{2}\left\{1 - \frac{\frac{1}{T}\left|\int_0^T \overrightarrow{\mathrm{WSS}} \, dt\right|}{\frac{1}{T}\int_0^T \left|\overrightarrow{\mathrm{WSS}}\right| \, dt}\right\}. \quad (4)$$

To quantify the helical behavior of blood flow, an index called Localized Normalized Helicity (LNH) was used:

$$\mathrm{LNH}_{(x,t)} = \frac{u \cdot \omega}{|u| \cdot |\omega|}, \quad (5)$$

where $\omega$ is the vorticity vector.

## 3. Results

In this section, we report the numerical results obtained. Since it is after the systolic peak and during the systolic deceleration phase that flow patterns in BAV related aortas become clearly defined, fluid streamlines and velocity contour plots, as well as WSS magnitudes, are displayed at mid-deceleration phase.

### 3.1. Flow patterns

Streamlines (Figure 2) in the AA of the healthy patient are mainly parallel to the aortic wall in the proximal section. Downstream, the flow is skewed towards the inner curvature, associated with high velocities, something usually observed in bends. Low velocities are observed in the outer curvature.

Alternatively, BAV related aortas display a peripheral skewing of the main flow systolic jet towards the outer ascending aortic wall. This jet has higher velocities than in the healthy case, depending on the PS prescribed inlet velocities. The main jet accelerates

along the outer curvature of the AA, suffering deflection from the right-anterior to the left-anterior quadrants in patients K, M and L and from the right-anterior to the right-posterior quadrants in patient T. This corresponds to a nested helical behavior, associated with the development of vortices which are PS: in patient L, even though turbulent low velocity flow is observed in the inner AA, no evident formation of helical behavior is displayed; in patient T, low velocity streamlines in swirling motion that extend from the inner curvature of the AA to the proximal DA are observed; in dilated aortas (patients M and K), we have peripheral recirculating vortices with moderate velocities arising from the main systolic jet and reaching the inner AA curvature, while smaller, low velocity vortices fill the center of the AA. Helicity is increased with dilation: dilated aortas from BAV patients present higher helicity in the AA than non-dilated aortas and patient K displays even more helical behavior than patient M. Nonetheless, with the ongoing of the cardiac cycle through late systole and diastole, helices are set throughout the aorta in all patients. Such feature shows that higher helicity is associated with AD and might have an important role towards its development and progression.

Regarding the MFS patient, blood recirculation is exaggerated at the aortic root owing to its dilation. Moreover, the arch coarctation present in this patient and patient L sets a recirculating behavior downstream.

### 3.2. WSS distributions

The WSS magnitude distribution is shown to be highly correlated with the flow streamlines and respective velocity field. At peak systole, the healthy aorta presents a relatively moderate WSS distribution in the proximal AA section, becoming asymmetric further downstream: due to the wall curvature and flow skewing towards the inner wall, an area of high WSS (maximum of 118 dyn/cm$^2$) appears in the beginning of the inner curvature of the AA, while lower WSS values are present on the outer wall. Such features are diminished, but still present during the deceleration phase (Figure 3). All BAV patients demonstrate delayed onset of peak systolic WSS, with maximum values of 170 dyn/cm$^2$, 276 dyn/cm$^2$, 126 dyn/cm$^2$ for patients M, K and L and a range from 300 to 500 dyn/cm$^2$ for patient T. Moreover, as observed in Figure 3, flow instability results in sites of increased systolic WSS in the outer curvature of the AA in all BAV patients, when compared with the healthy aorta. In addition, a wider WSS distribution is observed in the dilated aortas, which can be the result from the intense flow helicity predicted in BAV patients M and K versus that of patients L and T. Such hemodynamic disturbances suggest that the outer region of the AA is crucial for AD creation and development. Moreover, the recirculating vortices present in the AA of patients M and K result in fluctuations of systolic WSS on the middle section of the inner AA wall, with increased local WSS values in that region. At last, the dilated aortic root of the MFS patient presents very low WSS values, although locally increased WSS is observed at the upper portion of the root owing to the high helicity verified at this region.

### 3.3. Plane-wise analysis of TAWSS and OSI

TAWSS and OSI are analyzed at the mid-ascending aortic plane, or, for the patients with dilation, at the location of AD (Figures 5 and 6). In the healthy patient and BAV patients, maximum values of TAWSS are correlated with the sites characterized by the passage of high velocity systolic flow: in the former, high values are observed in the left-posterior quadrant due to the asymmetric flow observed at the AA curvature; in the latter, maximum values are observed at the quadrants corresponding to the outer curvature, owing to the systolic jet deflection. In the MFS patient, TAWSS resemble those of the healthy patient, showing that the flow helicity present in the dilated root exerts shear stress forces all around the dilated root. Oscillatory behavior is present in the healthy aorta, with bidirectional and nearly purely oscillatory flows owing to the AA curvature. Regarding BAV patients L and M, these present with a mainly unidirectional WSS at the wall area impinged by the valve jet; when moving away from that area, flow became oscillatory, except for patient M, where unidirectional WSS was also observed in the left-anterior quadrant. Such regions of high OSI corresponded well to regions of lower systolic TAWSS. In patient K, however, highly oscillatory behavior characterizes most of the quadrants, even in the region impinged by the valve jet. This suggests that the particular geometry of patient K might have influenced greatly flow deflection in comparison with the remaining BAV patients, causing an OSI overload. Finally, the MFS patient maintains a relatively low oscillatory flow in the dilated root, with mainly unidirectional WSS.

## 4. Discussion

This work demonstrates clearly that the aortic valve morphology induces notable flow abnormalities in the AA of BAV patients, in comparison with a normal TAV. Consistent with previous studies (Viscardi et al., 2010; Faggiano et al., 2012; Pasta et al., 2013; Rinaudo et al., 2014; Markl et al., 2011), and regardless of the shape of the AA, these FSI results show that the BAV gives rise to a peripheral skewing of the systolic jet towards the outer mid-ascending aortic wall, then accelerating along the outer curvature. Such hemodynamic behavior corresponds to an expected nested helical one, present in non-dilated and dilated aortas. Moreover, while in the healthy aorta helical flows started developing just at late systole and

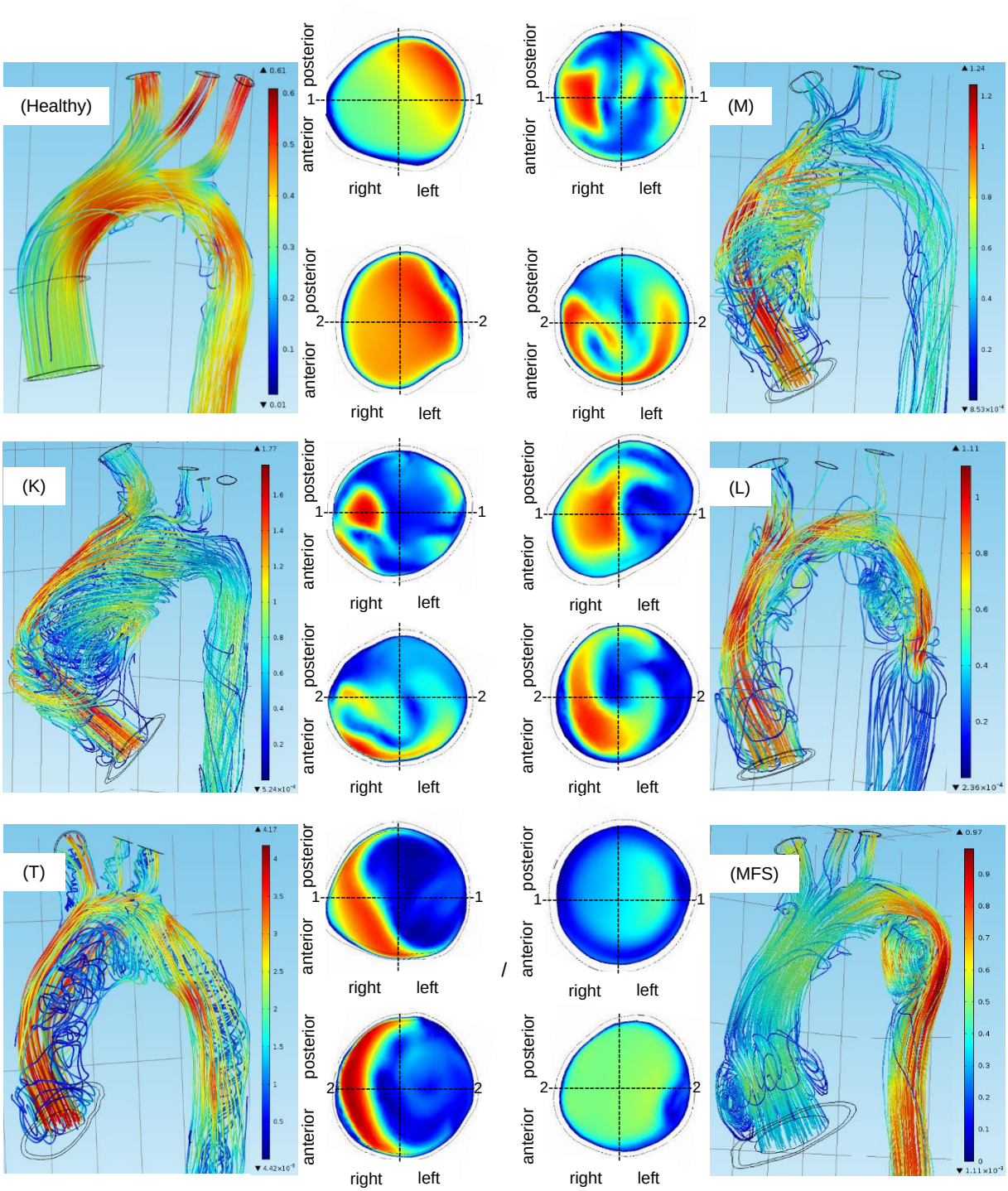


Figure 2 – Deceleration phase: velocity (m/s) and streamline fields are displayed for all patients. Regarding the velocity contour plots, the two from the left are associated with the streamline plot on the left and the two from the right are associated with the streamline plot on the right (1-1: middle section; 2-2: distal section).

through diastole, in BAV patients they originated at mid systole. Patient L, however, did not present evident helical behavior in the AA due to the straight AA geometry, although turbulent flow was observed. On the other hand, helices were intensified in dilated aortas from BAV patients, in agreement with the study from (Bonomi et al., 2015). Additionally, helicity was enhanced in the dilated root from the MFS patient, something corroborated by studies (Singh et al., 2016).

Flow abnormalities observed in the BAV patients also affected the WSS environment of the AA: strongly asymmetric WSS distributions along the AA were observed, with regions of stress overload in the outer curvature highly associated with the skewness of the BAV jet. Moreover, more marked WSS was found with increasing AD in these patients. Recent in vivo studies (Hope et al., 2010) have reported that BAV patients

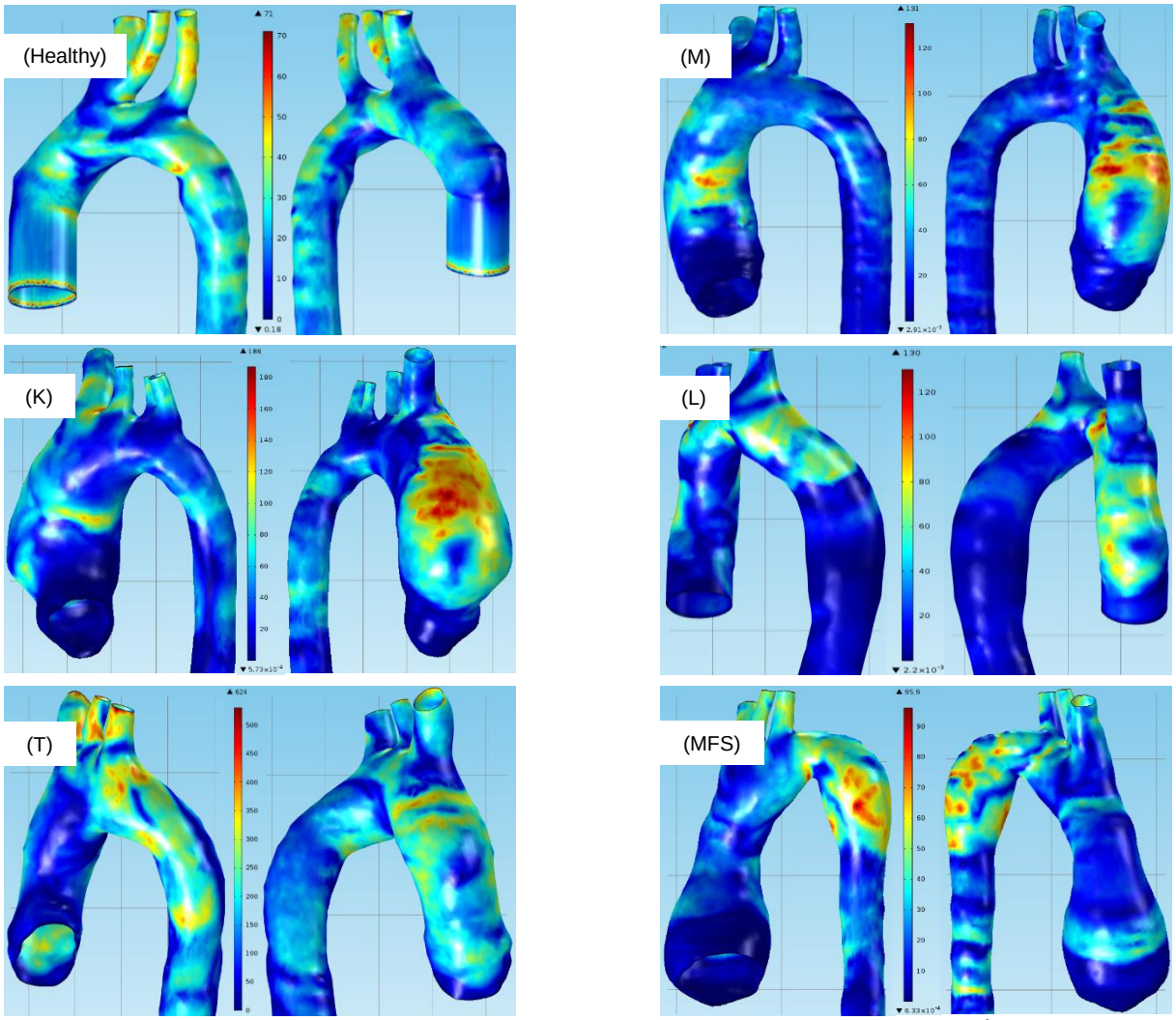


Figure 3 – Deceleration phase: WSS magnitude is displayed for all patients, in dyn/cm$^2$.

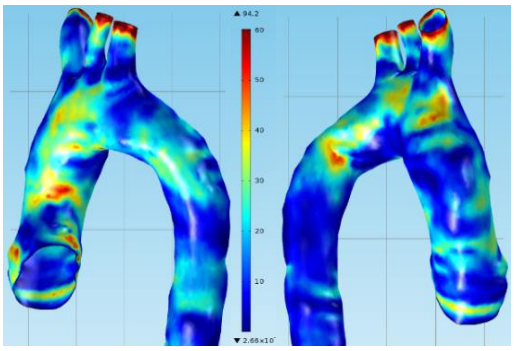

Figure 4 –WSS magnitude in the aorta of patient T, at late diastole, in dyn/cm$^2$.

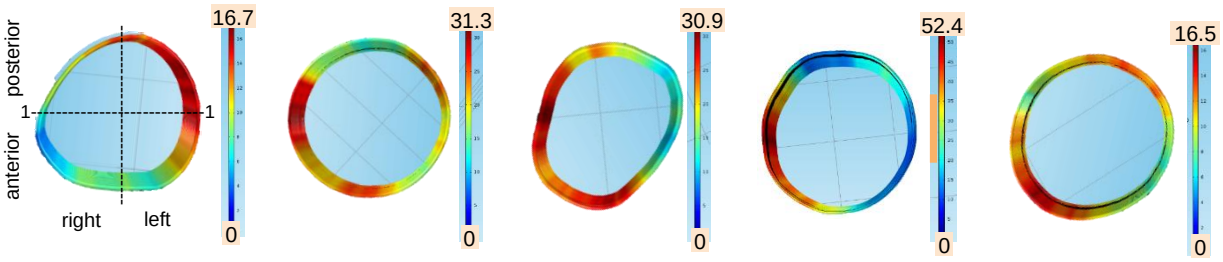


Figure 5 - TAWSS at the mid-ascending aortic plane (for all patients except the MFS patient) and at the root plane for the MFS patient, in dyn/cm$^2$. From left to right: healthy patient, BAV patients M, L and K, MFS patient.

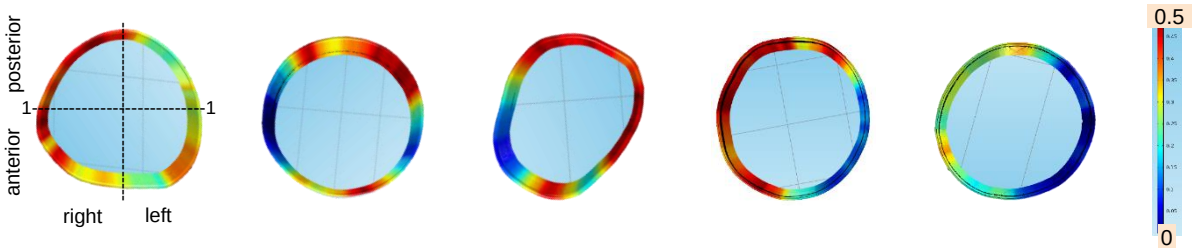


Figure 6 – OSI at the mid-ascending aortic plane (for all patients except the MFS patient) and at the root plane for the MFS patient. From left to right: healthy patient, BAV patients M, L and K, MFS patient.

present locally elevated systolic WSS on the outer dilated wall, as shown by this work.

The flow patterns and WSS distributions reported in this work for BAV patients therefore favor the hypothesis that underlying flow abnormalities play a direct role in the pathogenesis of BAV related aortopathies, namely the development of AD, and that this is not solely a genetic manifestation of connective tissue disorders. Indeed, WSS is an important vascular regulator that can induce vascular remodeling (Dolan et al., 2011) by directly influencing endothelial cell function. Therefore, the prolonged exposure of the outer curvature of the AA to altered WSS, associated with the high helicity present in BAV patients, may contribute to aortic degeneration and give rise to a more fragile vessel wall, inducing AD development.

Interestingly, a recent study recreated an *in vitro* flow system in an endothelial cell (cells covering the interface between blood and wall) culture 25 and found that very high WSS values (about 284 dyn/cm$^2$) increased cell apoptosis relative to lower WSS (35 dyn/cm$^2$) conditions, a biological event that occurs with vessel wall remodeling (Dolan et al., 2011). The values of peak-systolic WSS in patient K (with the greater AD) resemble those measured in cell culture by (Dolan et al., 2011). This study then suggests that very high WSS values may cause detrimental effects on the endothelial cell layer, causing mechanical damage to cell-cell junctions or cell surface integrity.

On the other hand, the WSS levels computed by all models in this work were systematically higher than those reported by *in vivo* measurements, where maximum WSS magnitudes of 23 dyn/cm$^2$ have been observed for BAV patients with AD (Rinaudo et al., 2014). However, the accuracy of MRI measurements is narrowed by low temporal and spatial resolutions of the order of 40 ms and 2 mm$^3$, respectively (Markl et al., 2011). Such features give rise to underestimated WSS estimations (Rinaudo et al., 2014). Several studies have shown that MRI is not currently able to provide accurate quantification of parameters such as WSS and thus computational modeling is advantageous in that matter (Boussel et al., 2009). Alternatively, our velocity and WSS results for BAV patients were in the same scale as those from (Rinaudo et al., 2014).

Alternatively, stress abnormalities generated by the BAV gave rise to a unidirectional WSS (low OSI) in patients M and L, corresponding to the region marked by the acceleration of the systolic jet, which contrasted with the bidirectional and oscillatory WSS distribution observed in the healthy patient. These observations suggest that the unidirectional environment on the outer wall of the AA in BAV patients could somehow trigger a local injury response causing the progressive degradation of the aortic wall. Nonetheless, in the healthy patient and BAV patients M and L, high OSI regions were also observed and well associated to regions of low TAWSS. Such correlation was associated with the development of atherosclerosis or ulcerating lesions in the aorta (Dolan et al., 2011; D'Ancona et al., 2013). Regarding BAV patient K, he shows elevated TAWSS associated with high OSI throughout the outer curvature of the AA, suggesting a fragile aortic wall.

While mild AR did not show any prejudicial effect in BAV patients L, M and K during diastole, severe AR caused important vascular changes in the aorta.

Patient T displayed high WSS values in the AA (more localized in the root) throughout diastole. This seems to demonstrate that severe AR and the associated abnormal hemodynamics do play a role in facilitating AD, especially in the aortic root, in agreement with the retrospective study from (Keane et al., 2000).

Alternatively, the dilated root from the MFS patient presented very low WSS values throughout the majority of the cardiac cycle, in agreement with the study from (Singh et al., 2016). In the computational study from (Boussel et al., 2008), PS models of intracranial aneurysms were highly associated with very low WSS distributions. This therefore shows that both very high and very low WSS values can be highly prejudicial towards the homeostasis of the vessel wall, since both can lead to processes of vessel wall remodeling (Dolan et al., 2011; Boussel et al., 2008). Thus, the obtained results for the MFS patient show that very low WSS in combination with increased helicity is associated with aortic root dilation, namely, aneurysm development. Moreover, such dilation derives from a combination between genetic and hemodynamic factors: the root wall is weakened due to vascular remodeling originated by connective tissue disorder and increased wall stiffness, which influences local hemodynamics towards the development of aortopathy (Aburawi et al., 2007; Singh et al., 2013).

## 5. Limitations and future work

The first limitation of this study concerns the creation of the aortic geometries: the segmentation procedure was challenging, because the CT images presented artifacts and low contrast between the aorta and the surrounding tissues. Thus, the images were of difficult interpretation and the segmentation process took longer than expected; plus, the model surface mesh simplification, although essential, retrieved characteristics from the original model. In the future, a more suitable process between image segmentation and geometry import to COMSOL needs further investigation.

Other limitations are related to the physical and computational models. First, the aortic blood was modeled as a laminar flow, which, even if allowing to assess the general hemodynamics in the AA during most of the cycle, is inaccurate at peak systole and in the early deceleration phase (Cao et al., 2015). Therefore, a turbulence or transition model should be considered (Bonomi et al., 2015). Finding a proper turbulence model for aortic flow remains a current open problem (Viscardi et al., 2010). Additionally, the aortic wall was assumed as an isotropic material, although it presents an anisotropic behavior.

On the other hand, the mesh densities used in numerical simulations were not ideal, since they had a relatively high error associated. However, this choice was necessary due to computational costs associated with FSI and work time available, since denser meshes would give rise to simulation running times higher than 7 or 8 days, which was impracticable. A recent research line in Cardiovascular Mathematics has been exploring the integration of simulation and data extracted by four-dimensional imaging methods (Piccinelli et al., 2010): such procedure, called data assimilation, involves tracking of the vessel wall motion and presents an interesting alternative to usual FSI. This reduces the associated computational cost and, when optimized, will be able to improve both the knowledge extracted from medical imaging data and the accuracy of numerical results.

Alternatively, the valve was modeled by the GOA and inflow conditions, and so opening and closing mechanisms, as well as the influence of leaflets, were not taken into account. Although in systole this approximation is sufficiently valid, in diastole it is not accurate. As future work, numerical modelling of the aortic structure with the valve orifice changing through time based on data obtained from MRI should be considered. Such subject was investigated in the work from (Wendell et al., 2013), where a time-varying mask of the valve inflow was used having into account the valve orifice segmented at several times during systole. The use of such method in the study of AD hemodynamics in BAV patients would be enlightening in both systole and diastole. Moreover, more research regarding numerical modeling of AR should be performed: since in this work the final conclusions to withdraw on this subject are qualitative, the exploration of this pathology should be ensured, especially when joined with BAV.

Finally, the inclusion of valve leaflets in BAV related numerical modeling should be investigated. It was previously observed that these do alter AA hemodynamics, highlighting the abnormalities of BAV flow (Bonomi et al., 2015). Therefore, even though the BAV orifice shape in combination with the aortic geometry is enough to recreate BAV related hemodynamics in the AA, research towards the inclusion of the valve leaflets should be considered.

## 6. Conclusions

In this work, we provided a deeper insight on the hemodynamics in the AA in diverse PS cases. Mainly, we demonstrated the altered hemodynamics and WSS distributions associated with BAV, with and without dilation, and in MFS. We can conclude that the estimation of vascular parameters (such as the WSS) through numerical modeling provides valuable biomarkers for the accurate description of the hemodynamic environment in diverse aortic pathologies. Nonetheless, every clinical case is different, and in BAV patients, the progress of aortopathy is usually unpredictable and we should not

generalize the conclusions from the numerical results obtained for a small group of patients.

We can conclude that, although this work presents several limitations, it allowed to study blood hemodynamics in BAV and MFS related pathologies. Mathematical modeling and numerical simulations of cardiovascular problems is a very promising research field that aims at obtaining the most accurate models and numerical results, motivated by the fact that cardiovascular diseases have a major impact in developed countries.

## References


Aburawi, E., O'Sullivan, J. (2007). Relation of aortic root dilatation and age in Marfan's syndrome. *European Heart Journal* 28: 376-379.

Barker, A., Lanning, C., Shandas, R. (2010). Quantification of Hemodynamic Wall Shear Stress in Patients with Bicuspid Aortic Valve Using Phase-Contrast MRI. *Ann Biomed Eng*. 38(3): 788–800.

Bonomi, D., Vergara, C., Faggiano, E., et al. (2015). Influence of the aortic valve leaflets on the fluid-dynamics in aorta in presence of a normally functioning bicuspid valve. Biomech Model Mechanobiol 14(6): 1349-61

Boussel, L., Rays, V., McCuloch, C., et al. (2008). Aneurysm growth occurs at region of low wall shear stress: Patient-specific correlation of hemodynamics and growth in a longitudinal study. *Stroke* 39(11): 2997-3002

Boussel, L., Rays, V., Martin, A., et al. (2009). Phase-contrast magnetic resonance imaging measurements in intracranial aneurysms in vivo of flow patterns, velocity fields, and wall shear stress: comparison with computational fluid dynamics. *Magn Reson Med.* 61(2): 409-17.

Cao, K., Sucosky, P. (2015). Effect of Bicuspid Aortic Valve Cusp Fusion on Aorta Wall Shear Stress: Preliminary Computational Assessment and Implication for Aortic Dilation. *World Journal of Cardiovascular Diseases* 5: 129-140

D'Ancona, G., Amaducci, A., Rinaudo, et al. (2013). Haemodynamic predictors of a penetrating atherosclerotic ulcer rupture using fluid-structure interaction analysis. *Interactive Cardiovascular and Thoracic Surgery* 17: 576-578.

Dolan, J. M., Meng, H., Singh, S., et al. (2011). High fluid shear stress and spatial shear stress gradients affect endothelial proliferation, survival, and alignment. *Ann Biomed Eng* 2011 39(6): 1620-31.

Erbel, R., Eggebrecht, H. (2006). Aortic dimensions and the risk of dissection. *Heart*, 92: 137–142.

Faggiano, E., Antiga, L., Puppini, G., et al. (2012). Helical flows and asymmetry of blood jet in dilated ascending aorta with normally functioning bicuspid valve. *Biomech Model Mechanobiol,* 12(4), 801-813

Hope, M., Hope, T., Meadows, A., et al. (2010). Bicuspid Aortic Valve: Four-dimensional MR Evaluation of Ascending Aortic Systolic Flow Patterns. *Radiology* 255(1): 53-61.

Janela, J., Moura, A., Sequeira, A. (2010). Absorbing boundary conditions for a 3D non-Newtonian fluid-structure interaction model for blood flow in arteries. *International Journal of Engineering Science*. 48: 1332–1349

Kang, J., Song, H., Yang, D., et al. (2013). Association Between Bicuspid Aortic Valve Phenotype and Patterns of Valvular Dysfunction and Bicuspid Aortopathy. *JACC: Cardiovascular Imaging* 6(2): 150-61.

Keane, M., Wiegers, S., Plappert, T., et al. (2000). Bicuspid Aortic Valves Are Associated With Aortic Dilatation Out of Proportion to Coexistent Valvular Lesions. Circulation 102: Iii-35-Iii-39.

Markl, M., Kilner, P., Ebbers, T. (2011). Comprehensive 4D velocity mapping of the heart and great vessels by cardiovascular magnetic resonance. *Journal of Cardiovascular Magnetic Resonance* 13(7): 1-22

Nagel, E., Rossum, A., Fleck, E. (2004). Cardiovascular Magnetic Resonance (1st ed.). Springer

Olufsen, M., Kim, W., Pedersen, E., Nadim, A., Larsen, J. (2000). Numerical Simulation and Experimental Validation of Blood Flow in Arteries with Structured-Tree Outflow Conditions. *Annals of Biomedical Engineering*. 28: 1281–1299

Pasta, S., Rinaudo, A., Luca, A., et al. (2013). Difference in hemodynamic and wall stress of ascending thoracic aortic aneurysms with bicuspid and tricuspid aortic valve. *Journal of Biomechanics*, 46(10), 1729-1738.

Piccinelli, M., Mirabella, L., Passerini, et al. (2010). 4D Image-Based CFD Simulation of a Compliant Blood Vessel. Emory University – Mathematics and Computer Science Department. 26 p. Technical Report TR-2010- 027

Reijer, P., Sallee, D., Velden, P., et al. (2010). Hemodynamic predictors of aortic dilatation in bicuspid aortic valve by velocity-encoded cardiovascular magnetic resonance. *Journal of Cardiovascular Magnetic Resonance* 12(4).

Rinaudo, A., Salvatore, P. (2014). Regional variation of wall shear stress in ascending thoracic aortic aneurysms. *Proc IMechE Part H: J Engineering in Medicine* 1-12.

Singh, S., Xu, X., Wood, N., et al. (2016). Aortic flow patterns before and after personalised external aortic root support implantation in Marfan patients. *Journal of Biomechanics* 49(1): 100-111

Tilea, I., Suciu, H., Tilea, B., et al. (2013). Anatomy and Function of Normal Aortic Valvular Complex. Chapter 2 of *Calcific Aortic Valve Disease*.

Viscardi, F., Vergara, C., Antiga, L., et al. (2010). Comparative Finite Element Model Analysis of Ascending Aortic Flow in Bicuspid and Tricuspid Aortic Valve. *Artificial Organs* 34(12): 1114-1120.

Wendell, D., Samyn, M., Cava, J., et al. (2013). Including aortic valve morphology in computational fluid dynamics simulations: Initial findings and application to aortic coarctation. *Medical Engineering & Physics* 35: 723-735